

Observation of charge-density-wave excitations in manganites

A. Nucara¹, P. Maselli¹, P. Calvani¹, R. Soprocase¹, M. Ortolani²,
G. Gruener³, M. Cestelli Guidi⁴, U. Schade², and J. García⁵

¹*CNR-INFM Coherencia and Dipartimento di Fisica,*

Università di Roma La Sapienza, Piazzale A. Moro 2, I-00185 Roma, Italy

²*Berliner Elektronenspeicherring-Gesellschaft für Synchrotronstrahlung m.b.H.,*

Albert-Einstein Strasse 15, D-12489 Berlin, Germany

³*Laboratoire d'Electrodynamique des Matériaux Avancés,*

UMR 6157 CNRS-CEA, Université Francois Rabelais,

Parc de Grandmont, 37200 Tours, France

⁴*Laboratori Nazionali INFN di Frascati,*

Via E. Fermi 40, Frascati, I-00044 Italy and

⁵*Instituto de Ciencia de Materiales de Aragon and*

Departemento de Fisica de la Materia Condensada,

Consejo Superior de Investigaciones Cientificas y

Universidad de Zaragoza, 50009 Zaragoza, Spain

(Dated: August 19, 2021)

Abstract

In the optical conductivity of four different manganites with commensurate charge order (CO), strong peaks appear in the meV range below the ordering temperature T_{CO} . They are similar to those reported for one-dimensional charge density waves (CDW) and are assigned to pinned phasons. The peaks and their overtones allow one to obtain, for $\text{La}_{1-n/8}\text{Ca}_{n/8}\text{MnO}_3$ with $n = 5, 6$, the electron-phonon coupling, the effective mass of the CO system, and its contribution to the dielectric constant. These results support a description of the CO in La-Ca manganites in terms of moderately weak-coupling and of the CDW theory.

PACS numbers: 75.47.Lx, 78.20.Ls, 78.30.-j

The competition between the tendency of electrons to delocalize and the simultaneous presence of interactions like magnetism, Coulomb repulsion, and electron-phonon coupling is the origin of the extremely rich x, T phase diagram of manganites like $\text{La}_{1-x}\text{Ca}_x\text{MnO}_3$ (LCMO)¹. It also includes, for $0.5 \leq x < 0.85$ and below an ordering temperature T_{CO} , charge-order (CO) phases² which are usually associated with both orbital ordering and antiferromagnetism (AF). For a long time these phenomena were described in terms of stripes of localized charges, where the mixed valence of manganese is split³ between Mn^{+3} ions surrounded by Jahn-Teller-distorted O^{-2} octahedra and Mn^{+4} ions at undistorted sites. This strong-coupling scenario has been recently questioned on the basis of experiments which indicate⁴ charge disproportion < 1 , exclude strong localization⁵, and show⁶ that the charge modulation remains uniform when passing from commensurate to incommensurate doping. A collective sliding of the charge system was also observed, at $x = 0.5$, in not too strong electric fields⁷. All these results indicate that, in several manganites, the CO phase can be described⁸ in terms of the Charge Density Waves (CDW) model^{9,10}, which assumes weak electron-phonon coupling. This hypothesis might be tested by measuring the gap 2Δ which opens in the real part of the optical conductivity $\sigma(\omega)$ below T_{CO} . Indeed, $2\Delta(T \simeq 0)/T_{CO} = 3.53$ in the weak-coupling limit and increases with the charge-lattice interaction. However, different gap values are reported in the literature for similar compounds. They seem to depend on the quality of the samples, on the extrapolation to zero of the mid-infrared $\sigma(\omega)$, on the addition of a pseudogap^{11,12}.

Besides the single-particle excitation at $\omega > 2\Delta$, the CDW model predicts two collective modes¹⁰ at $\omega \ll 2\Delta$, the phason and the amplitudon. The former one is infrared active¹⁰ and its dispersion ω_p vs. k is acoustic-like, with $\omega_p(\vec{k} = 0) = \Omega_p = 0$. However, either if the CDW is pinned to lattice impurities, or it is commensurate with the lattice¹⁰, the phason moves to $\Omega_p > 0$. The amplitudon is Raman active and its $\omega_a(\vec{k})$ is similar to that of an optical phonon, with $\omega_a > \omega_p$ for any \vec{k} . Pairs of such peaks were indeed detected at meV energies in one-dimensional conductors like the "blue bronze" family¹³ $\text{K}_{0.3}\text{Mo}_{1-x}\text{W}_x\text{O}_3$. The lowest-energy member of the pair was assigned to the pinned phason, the other one to a "collective bound resonance" due to the interaction between the collective mode itself and the impurities. The authors reported for the CDW an effective mass m^*/m_b varying from 700 to 800, where m_b is the one-electron band mass.

In the manganite family one has the opportunity to study the excitation spectrum of

TABLE I: Transition temperatures T_{CO} (from the literature) and charge-order parameters of four manganites at 10 K (from the present experiment). The symbols are explained in the text.

Sample	T_{CO} (K)	Ω_p (cm^{-1})	Ω_a (cm^{-1})	λ	ϵ_0^{CDW}	$\epsilon_{0,calc}^{CDW}$	m^*/m_b
$\text{Nd}_{1/2}\text{Sr}_{1/2}\text{MnO}_3$	150 ¹⁸	5.5					
$\text{La}_{3/8}\text{Ca}_{5/8}\text{MnO}_3$	270 ¹⁶	10.5 - 14.5	40	0.7	100	90	400
$\text{La}_{1/4}\text{Ca}_{3/4}\text{MnO}_3$	230 ¹⁶	7.5	30	0.8	150	120	700
$\text{La}_{1/8}\text{Ca}_{7/8}\text{MnO}_3$	130-150 ^{16,19}	8.5					

a multi-dimensional CDW. However, to our knowledge, experimental results have been reported up to now for $\text{Pr}_{0.7}\text{Ca}_{0.3}\text{MnO}_3$ only. By using time-domain THz spectroscopy¹⁴, both a peak at 25 cm^{-1} and a broad shoulder at lower frequencies were detected, and attributed to CDW collective excitations. The fact that both features survived at temperatures much higher than T_{CO} was justified in terms of charge-order fluctuations on a local scale¹⁴.

In the present paper we study, down to frequencies ω_{min} which range from 4.5 to 10 cm^{-1} , the optical conductivity of four manganites. One of them is a $\text{Nd}_{1/2}\text{Sr}_{1/2}\text{MnO}_3$ (NSMO) single crystal, grown and characterized as described in Ref. 5, and here measured in the ab plane. The other ones are polycrystalline pellets of $\text{La}_{1-n/8}\text{Ca}_{n/8}\text{MnO}_3$ with $n = 5,6,7$, namely with doping values where large single crystals are difficult to grow¹². They were obtained by an organic gel-assisted citrate process¹⁷, and controlled by X-ray powder diffraction. A further check on the sample with $n = 5$ showed the expected change of slope in the resistivity at $T_{CO} = 270 \text{ K}$. Both NSMO and the LCMO's with $n = 5,6$ are pseudocubic and, below T_{CO} , in a highly symmetric AF phase (CE)¹⁶. Therein, $\sigma(\omega)$ was found to be independent of the crystal direction below 1 eV ¹⁵. Therefore, the ab -plane conductivity of NSMO can be correctly compared with that of the randomly oriented LCMO crystallites. In the case of $n = 7$ the AF phase associated with the CO is uniaxial. However the structure is monoclinic and, even if a single crystal were available, the response of different axes could hardly be separated. As shown in Table I the four compounds have much different T_{CO} , in order to establish a sound relation between the observed spectral features and their CO phases.

The reflectivity $R(\omega)$ of all samples was measured at nearly normal incidence, after accurate polishing with sub-micron-thick powders. The sample thickness (2 mm) was such that

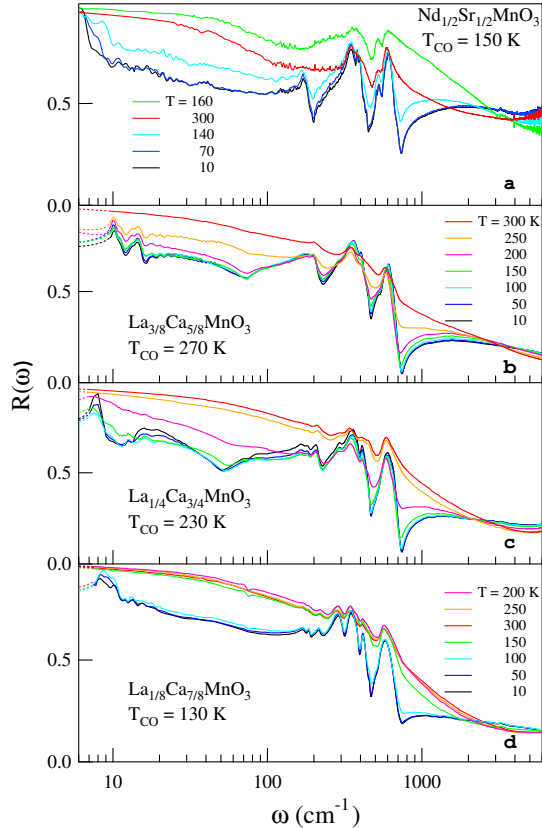


FIG. 1: Color online. Reflectivity at different temperatures of the single crystal of $\text{Nd}_{1/2}\text{Sr}_{1/2}\text{MnO}_3$ and of the polycrystalline pellets of $\text{La}_{1-n/8}\text{Ca}_{n/8}\text{MnO}_3$. The dashed lines show the Drude-Lorentz extrapolations of $R(\omega)$ from ω_{min} to $\omega = 0$.

interference fringes due to multiple reflections were negligible. However, their presence both in the single crystal (Fig. 1-a) and in the sample of Fig. 1-b, shows that the pellets are optically homogeneous at long wavelengths. The conventional radiation sources used between 20 and 6000 cm^{-1} were replaced by the Coherent Synchrotron Radiation (CSR) of the BESSY storage ring²⁰ from ω_{min} to 30 cm^{-1} , by just rotating the entrance mirror of the interferometer. In the meV range $R(\omega)$ was thus measured²¹ with a 1% error at a resolution of 0.5 cm^{-1} . The samples were thermalized in a He-flow cryostat within $\pm 2\text{ K}$, between 300 and 10 K. The reference was the sample itself, coated with a gold film evaporated *in situ*. $R(\omega)$ was extrapolated to $\omega = 0$ by accurate Drude-Lorentz fits and $\sigma(\omega)$ was obtained by standard Kramers-Kronig transformations.

The reflectivity of the four samples is shown in Fig. 1. All spectra show the transition to an insulating state below T_{CO} , with the opening of an infrared gap and the appearance of

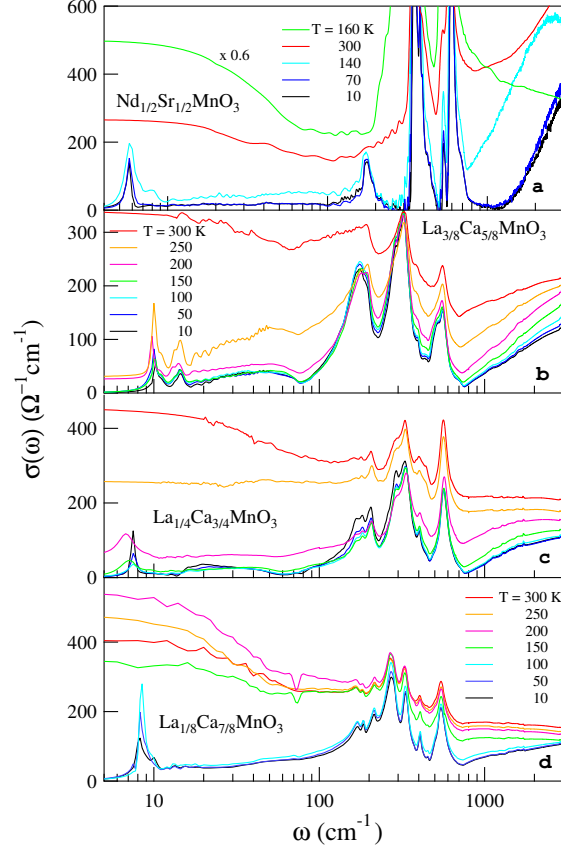


FIG. 2: Color online. Optical conductivity at different temperatures of the single crystal of $\text{Nd}_{1/2}\text{Sr}_{1/2}\text{MnO}_3$ and of the polycrystalline pellets of $\text{La}_{1-n/8}\text{Ca}_{n/8}\text{MnO}_3$.

strong phonon bands. The $R(\omega)$ of NSMO in Fig. 1-a is intermediate between that reported for a polished crystal and that of a cleaved crystal²². Below T_{CO} , in all samples of Fig. 1 one also observes novel spectral features in the meV range. The lowest-frequency feature is a sharp increase in R , by 10% to 20 %, around 10 cm^{-1} . In NSMO (Fig. 1-a), it might indicate a very narrow free-carrier absorption. However, this was ruled out after considering both that the dc conductivity²² of $\text{Nd}_{1/2}\text{Sr}_{1/2}\text{MnO}_3$ is vanishingly small at low T , and that one cannot fit its $R(\omega)$ to a Drude term at low ω . A comparison with the peaks of the other three samples in Fig. 1 suggests that also NSMO has a peak at finite frequency, whose low-energy side is not seen because it is beyond ω_{min} . In the La-Ca manganites a broad absorption is also detected below 100 cm^{-1} , with the same T -dependence as the main peak. At T_{CO} all the low- ω features disappear. This is not due to a shielding effect of the free carriers which, around T_{CO} , neither screen the phonons nor their weak shoulders.

The optical conductivity of the four samples, shown in Fig. 2, exhibits a weak Drude term above T_{CO} . In NSMO, which at $T > T_{CO}$ is ferromagnetic metallic, $\sigma(\omega)$ increases upon heating, to decrease again above the Curie temperature $T_c \simeq 225$ K (Fig. 2-a). Below T_{CO} an optical gap 2Δ opens in the $\sigma(\omega)$ of all samples. By smooth extrapolations of the lowest- T curves to $\sigma = 0$, one finds $2\Delta(T \simeq 0) \sim 800 \text{ cm}^{-1}$ or 0.1 eV in the polycrystalline samples of LCMO, ~ 0.2 eV in NSMO. Correspondingly, sharp conductivity peaks appear at the lowest frequencies in all panels of Fig. 2. Single peaks are observed in $\text{Nd}_{1/2}\text{Sr}_{1/2}\text{MnO}_3$ (Fig. 2-a), where the CO is homogeneous with periodicity $\Lambda = 2a$ ($a =$ lattice constant), in $\text{La}_{1/4}\text{Ca}_{3/4}\text{MnO}_3$ (c) where $\Lambda = 4a^1$, and in $\text{La}_{1/8}\text{Ca}_{7/8}\text{MnO}_3$ (d) where Λ is not known. Two well resolved peaks appear instead in $\text{La}_{3/8}\text{Ca}_{5/8}\text{MnO}_3$ (Fig. 2-b), where electron diffraction shows a coexistence of $\Lambda = 2a$ (25%) and $\Lambda = 3a$ (75%)¹. The peak width increases with T in a) and c), as expected, but neither in b) nor in d). These discrepancies may be attributed to the uncertainty in the extrapolation of $R(\omega)$ to $\omega = 0$ and to the changes with T of the background reflectivity. We assign the peaks in the meV range to phasons in a "pinned state", consistently with the presence in our samples of both impurities and commensurability. Their frequencies Ω_p (see Table I) are all larger than in¹³ $\text{K}_{0.3}\text{MoO}_3$ (3.3 cm^{-1}) and, in the three samples with CE-type charge order, are found to scale with T_{CO} .

The broad band observed in the La-Ca compounds at $\omega > \Omega_p$ approximately follows the T -dependence of the phason peak and disappears into the Drude continuum above T_{CO} . In $\text{La}_{1/4}\text{Ca}_{3/4}\text{MnO}_3$ (Fig. 3) it is shown to be the sum of two contributions. One of them broadens with T like the phason peak at 7.5 cm^{-1} , while the other one is nearly T -independent. A similar fit was obtained for $\text{La}_{3/8}\text{Ca}_{5/8}\text{MnO}_3$. We assign those two features to the overtone $2\omega_p$ and to a phason-amplitudon combination band $\omega_p + \omega_a$, respectively, basing on the following arguments: i) the CDW theory, once developed to the second order, implies a phase-amplitude mixing⁹; ii) a combination phason + amplitudon is expected to be infrared active (as its irreducible representation should include that of the phason); iii) the T -dependent peak shows at 10 K a sharp edge at $\simeq 12 \text{ cm}^{-1}$, a value consistent with the minimum overtone frequency, $2\Omega_p - \delta_{2p}$, for a reasonable anharmonic shift $\delta_{2p} \simeq 3 \text{ cm}^{-1}$; iv) the frequency predicted for the amplitudon at moderately weak coupling is $\sim 5 \text{ meV}^{10}$ or $\sim 40 \text{ cm}^{-1}$; v) the amplitudon should be more robust vs. the loss of coherence with temperature than the phason; vi) both the overtone and the combination band are expected to be broad, as their frequencies result from any combination of wavevectors \vec{k}_p and $\vec{k}'_{a(p)}$,

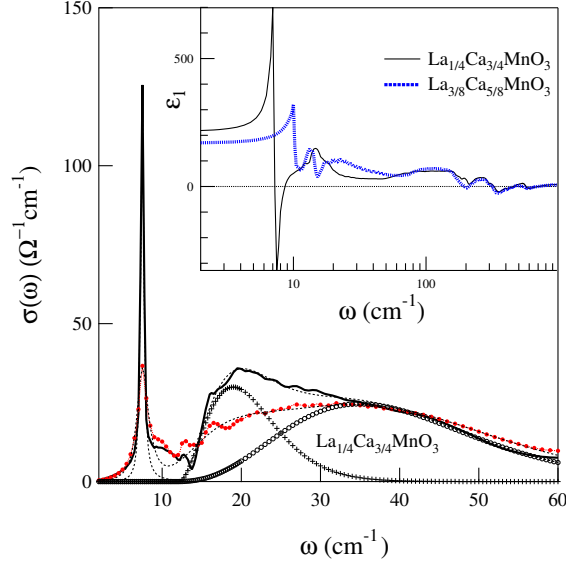


FIG. 3: Color online. Low-energy conductivity of $\text{La}_{1/4}\text{Ca}_{3/4}\text{MnO}_3$ at 10 K (solid line) and 100 K (dots) with the corresponding best fits (thin-dotted lines). The side band is the sum of the overtone $2\Omega_p$ and of the combination band $\Omega_p + \Omega_a$, as shown at 10 K by crosses and open circles, respectively. The inset shows the CDW contribution to the real part of the dielectric function $\epsilon_1(\omega)$ in two samples at 10 K.

provided that $\vec{k}_p + \vec{k}'_{a(p)} \simeq 0$. Similar bands are observed in the vibrational overtones of molecular crystals²³.

Both the pinned-phason mode and the amplitudon have a nearly flat dispersion, then a high density of states, close to $\vec{k}_a = 0$. If therefore $\omega_p + \omega_a$ is peaked at $\Omega_p + \Omega_a$, and $\delta_{p+a} \simeq \delta_{2p}$, one obtains the values of Ω_a reported in Table I for $x = 5/8$ and $3/4$ (where the side band is better resolved). They allow us to obtain a first description of the CO phase in manganites, including the electron-phonon interaction strength λ . For $\vec{k} = 0$ one has¹⁰

$$\Omega_a^2 = \lambda\omega^2(2k_F), \quad (1)$$

where $\omega(2k_F)$ is the acoustic-phonon frequency at twice the Fermi wavevector. Here, for the CDW at $x = 3/4$ ($5/8$) with period¹ $4a$ (mainly $3a$), $2k_F = \pi/2a$ ($2\pi/3a$). Calculations of the acoustic branches²⁴ in LaMnO_3 provide $\omega(2k_F) = 36$ (48) cm^{-1} , which gives $\lambda \simeq 0.8$ (0.7). The assumptions of the CDW model are thus justified *a posteriori*, independently of the evaluation of Δ and of its large uncertainty. The effective mass of the CDW is instead

very sensitive to the gap value. Using Eq. 1, it can be written¹⁰ as

$$\frac{m^*}{m_b} \simeq \left[\frac{2\Delta}{\Omega_a} \right]^2, \quad (2)$$

With the present $2\Delta \sim 0.1$ eV or 800 cm^{-1} one obtains $m^*/m_b \simeq 400$ (700) for $x = 5/8$ (3/4) at 10 K, to be compared with $m^*/m_b \simeq 800$ reported for the one-dimensional CDW of $\text{K}_{0.3}\text{MoO}_3$ ¹³.

Equation 2 can also be used to theoretically predict another parameter which can be directly measured: the CDW contribution to the dielectric constant ϵ_0^{CDW} . As here ω_{min} is lower than any CDW absorption, the experimental $\epsilon_1(\omega_{min})$ at low T measures ϵ_0^{CDW} , after one subtracts the phonon contributions and the high-frequency term ϵ_∞ . From the inset of Fig. 3 we thus obtain $\epsilon_0^{CDW} = 100$ (150) at $x = 5/8$ (3/4). These results can be compared with Eq. 3.22 of Ref. 10, that we write as

$$\epsilon_{0,calc}^{CDW} = 1 + \epsilon_{0,comb} + \left(\frac{\Omega_{pl}}{2\Delta} \right)^2 \left[\left(\frac{\Omega_a}{\Omega_p} \right)^2 + 4 \right]. \quad (3)$$

Therein, we have assumed that all carriers condense into the CDW ground state at $T \ll T_{CO}$ and we have added the contribution $\epsilon_{0,comb}$ of the combination band. In Eq. 3 one has $2\Delta \sim 800 \text{ cm}^{-1}$, a plasma frequency $\Omega_{pl} (T = 300 \text{ K}) = 1200$ (1540) cm^{-1} , $\epsilon_{0,comb} = 34$ (36) for LCMO with $x = 5/8$ (3/4). By also using the Ω_p and Ω_a values of Table I, one obtains $\epsilon_{0,calc}^{CDW} = 90$ (120) at $x = 5/8$ (3/4) in very good agreement with the experimental ϵ_0^{CDW} reported above.

In conclusion, we have first explored in the meV range the optical conductivity of four manganites with different T_{CO} , by using a coherent synchrotron source. We have found sharp peaks which disappear above T_{CO} and are similar to those reported for one-dimensional CDW's. They have been assigned to pinned phasons, followed by broad combinations of phasons and amplitudons. All parameters extracted from the spectra, like the electron-phonon coupling and the CO-phase contribution to the dielectric constant, are consistent with a description of the charge order in La-Ca manganites in terms of charge density waves, even at commensurate doping.

We wish to thank X. Blasco for providing the NSMO crystal.

- ¹ C. H. Chen and S.-W. Cheong, Phys. Rev. Lett. **76**, 4042 (1996); S. Mori, C. H. Chen, and S.-W. Cheong, Nature (London) **392**, 473 (1998).
- ² For a review, see E. Dagotto, T. Hotta, and A. Moreo, Phys. Rep. **344**, 1 (2001).
- ³ J. Goodenough, Phys. Rev. **100**, 564 (1955).
- ⁴ G. Subias, J. García, M. G. Proietti, and J. Blasco, Phys. Rev. B **56**, 8183 (1997); J. Garca *et al.*, J. Phys. Condensed Matter **13**, 3229 (2001).
- ⁵ J. Herrero-Martin, J. García, G. Subias, J. Blasco, and M. Concepcion Sanchez, Phys. Rev. B **70**, 024408 (2004).
- ⁶ J. C. Loudon *et al.*, Phys. Rev. Lett. **94**, 097202 (2005).
- ⁷ S. Cox *et al.*, Nature Materials **7**, 25 (2008).
- ⁸ G. C. Milward, M. J. Calderón, and P. B. Littlewood, Nature (London) **433**, 607 (2005).
- ⁹ P. A. Lee, T. M. Rice, and P. W. Anderson, Solid State Commun. **14**, 703 (1974).
- ¹⁰ G. Grüner, Rev. Mod. Phys. **60**, 1129 (1988).
- ¹¹ P. Calvani *et al.*, Phys. Rev. Lett. **81**, 4504 (1998).
- ¹² M.W. Kim *et al.*, Phys. Rev. Lett. **89**, 016403 (2002).
- ¹³ L. Degiorgi and G. Grüner, Phys. Rev. B **44**, 7820 (1991).
- ¹⁴ N. Kida and M. Tonouchi, Phys. Rev. B **66**, 024401 (2002).
- ¹⁵ K. Tobe, T. Kimura, and Y. Tokura, Phys. Rev. B **69**, 014407 (2004).
- ¹⁶ M. Pissas and G. Kallias, Phys. Rev. B **68**, 134414 (2003).
- ¹⁷ A. Douy and P. Odier, Mat. Res. Bull. **24**, 1119 (1989).
- ¹⁸ Yu. F. Popov *et al.*, Phys. Solid State **45**, 1221 (2003).
- ¹⁹ X. G. Li *et al.*, Europhys. Lett. **60**, 670 (2002).
- ²⁰ M. Abo-Bakr *et al.*, Phys. Rev. Lett. **90**, 094801 (2003).
- ²¹ M. Ortolani *et al.*, Phys. Rev. Lett. **97**, 097002(2006).
- ²² K. Takenaka, S. Okuyama, S. Sugai, and M. Yu. Maksimuk, J. Phys. Soc. Japan, **71**, 3065 (2002).
- ²³ P. Calvani, S. Cunsolo, and S. Lupi, J. Chem. Phys. **44**, 4650 (1991).
- ²⁴ E. G. Rini, M. N. Rao, S. L. Chaplot, N. K. Gaur, and R. K. Singh, Phys. Rev. B **75**, 214301

(2007).